Degradation of AlSi10Mg powder during laser based powder bed fusion processing

Materials and Design 198 (2021) 109358

Contents lists available at ScienceDirect

Materials and Design

journal homepage: www.elsevier.com/locate/matdes

Degradation of AlSi10Mg powder during laser based powder bed fusion processing

Ahmad Raza [a,*], Tobias Fiegl [b], Imran Hanif [c], Andreas MarkstrÖm [d], Martin Franke [b], Carolin Körner [e], Eduard Hryha [a]

[a] Department of Industrial and Materials Science, Chalmers University of Technology, Gothenburg SE-41296, Sweden
[b] Neue Materialien Fürth GmbH, Dr.-Mack-Str. 81, Fürth 90762, Germany
[c] Department of Chemistry and Chemical Engineering, Chalmers University of Technology, Gothenburg SE-42196, Sweden
[d] Thermo-Calc Software AB, Råsundavägen 18, 169 67, Stockholm, Sweden
[e] Materials Science and Engineering for Metals, Friedrich-Alexander Universität Erlangen-Nürnberg, Martensstraße 5, 91058, Germany

HIGHLIGHTS

- The volume fraction of spatter particles increased up to 3% in the powder used for 30 months.
- The surface of spatter particles showed presence of thick (up to 120 nm) oxide columnar scale.
- Enrichment in Mg-base oxide was observed with the ageing
- Average oxide layer thickness increased by almost an order of magnitude after 30 months of reuse.

GRAPHICAL ABSTRACT

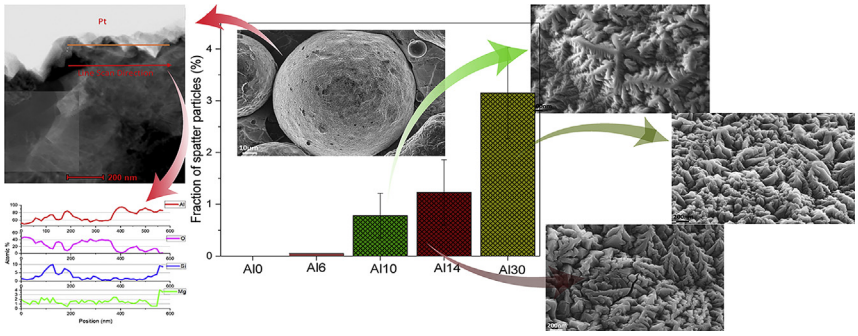

ARTICLE INFO

Article history:
Received 26 October 2020
Received in revised form 15 November 2020
Accepted 23 November 2020
Available online 24 November 2020

Keywords:
Additive manufacturing
Laser based powder bed fusion
Powder degradation
Reused powder in AM
Spatter particles
AlSi10Mg powder

ABSTRACT

Knowledge concerning powder degradation during additive manufacturing (AM) processing is essential to improve the reusability of the powder in AM and hence maximize feedstock powder reuse and economy of the process. AlSi10Mg powder degradation in Concept Laser XLINE 2000R machine over the total period of 30 months was analyzed in order to understand the extent and mechanism affecting powder aging. Thereby, detailed analysis of the powder morphology, microstructure and surface chemistry was performed by SEM, TEM and XPS. The results show an increase in volume fraction of heavily oxidized spatter particles up to 3% in 30 months. XPS analysis of the powder surface chemistry indicates that powder particles are covered by uniform oxide layer, formed by Mg- and Al-based oxides, average thickness of which increased from ~4 nm in case of the virgin powder up to about 38 nm in case of the reused for about 30 month powder, established by XPS. Analysis of the oxide characteristics were consistent with the observed oxygen content in the sampled powder. Columnar oxide scale formation on spatter particles was revealed as well, reaching up to 125 nm in thickness measured using STEM. Results of the XPS and STEM-EDX analysis of oxide composition are shown to be in agreement with the thermodynamic calculations confirming that oxide scale on sputter particles is formed by $MgAl_2O_4$ spinel and Al_2O_3 (corundum) oxides.

1. Introduction

The challenges with the reuse of the powder in the powder bed fusion (PBF) techniques poses serious concerns about the cost reduction

* Corresponding author.
E-mail address: ahmadra@chalmers.se (A. Raza).

https://doi.org/10.1016/j.matdes.2020.109358

and sustainability of additive manufacturing (AM) process [1]. At the current state-of-the-art, due to the lack of knowledge concerning powder degradation, powder reuse is typically based on specific end-user internal procedures established on "best practice" approach. The reusability of powder varies based on the used PBF techniques from electron beam powder bed fusion (EB-PBF, most often referred to as electron beam melting (EBM)) to laser powder bed fusion (LB-PBF) given the variance in processing conditions. Among those, LB-PBF is frequently used in AM due to the variety of the alloys which can be processed including various steels, superalloys, Al- and Ti- alloys, etc. Commercially available AM process for Al alloys only exists for LB-PBF technique as it cannot be done in EBM due to higher metallization rate [2].

The AlSi10Mg possess good castability, weldability (essential for AM), hardenability, high corrosion resistance and keeps a good thermal conductivity [3,4]. Al-Si is a near eutectic alloy where the introduction of Mg causes Mg_2Si precipitation which strengthen the matrix without compromising the other mechanical characteristics. Considering good mechanical strength, high thermal conductivity and light weight, aerospace industry is utilizing this alloy through AM to achieve better geometrical design freedom [4]. LB-PBF is the common fabrication process where AlSi10Mg powder is used with size in range of 10-100 μm. Although the fabrication is mostly conducted at room temperature in LB-PBF or build plate preheating between 100 and 200°C, the powder degradation makes re-usability a challenging aspect particularly for AlSi10Mg as Al and Mg are highly reactive elements [5].

Principally, the quality of reused powder can be degraded by a couple of routes, including the powder oxidation (powder handling or during AM processing in the chamber) and spatters formation [1,6]. Powder oxidation is a commonly occurring phenomenon and mainly depends on the susceptibility of the elements to oxidation, environment conditions (temperature and atmosphere composition) and exposure time [7–9]. Hence, the alloys containing elements with high oxygen affinity as Al, Ti, etc. are highly prone to form oxide particulates or a uniform oxide layer over the surface of the powder particles. The thickness of oxide layer is determined by the build chamber environment, exposure time, and temperature. Considering LB-PBF, which usually is an ambient temperature process, it is less vulnerable to the significant powder surface oxidation. However, build plate preheating, typically up to 200°C in most industrially applied LB-PBF hardware, can bring some potential risk of powder degradation for sensitive alloys. Nevertheless, a more significant way of powder degradation is the spatter formation during the built process. Numerous factors influence the generation of spatters during the processing, including beam energy density, beam size, scanning speed, type of alloy, processing gas and its purity, chamber environment, etc. [10–13] Typical oxygen level in LB-PBF chamber is around 1000 ppm of oxygen, meaning that oxygen potential in the chamber is pretty high and hence strongly oxidizing for the molten spatter particles [6,14].

Several researchers have comprehensively studied the mechanism of spatter formation using finite element modeling and ultrahigh-speed imaging [8,9,11]. The phenomenon is linked with the vaporization of molten metal and burst of bubble containing vapors which cause the formation of spatters by Leung et al. [10]. In another study, Gunenthriram et al. [15] has compared the spatter ejection mechanism from melt pool for 316L stainless steel and Al12Si where 316L stainless steel exhibited higher spatter generation compared to Al12Si, which has been connected to incorporation of ejected droplets in melt pool. Moreover, Gunenthiram et al. [15] found a direct relation between molten droplet ejection from melt pool and volumetric energy density (VED). A few researchers have taken a leap forward to examine the oxidation of spatters by morphological analysis and have conducted overall powder degradation analysis [16]. In a study on Hastelloy X, Gasper et al. evaluated the spatters formed in LB-PBF process and showed their influence on oxides incorporation in final product [1]. The study showed that 30-60% of spatter particles lies in similar size distribution as the rest of powder, and hence get reused and had a highly oxidized surface. The presence of such spatters can seriously degrade the properties of fabricated product.

Impact of powder reusability on fabricated parts is also studied by few researchers, both in LB-PBF and EB-PBF process. Ardila et al. [17] have observed no significant impact on product's properties after reusing IN718 powder in 14 cycles in LB-PBF. Contrarily, Gruber et al. [18] showed a substantial IN718 powder degradation and formation of Al based oxide on the surface in EB-PBF [7]. The difference has been stemmed from temperature difference in build chamber varying from room temperature in LB-PBF to around 1000°C in EB-PBF. Similar studies have been also conducted on 304L stainless steel and TiAl6V4 alloys where powder degradation has been observed in reused powder [19–22]. In powder degradation analysis, the sample exposure time in the machine was mostly limited to a few reusability cycles, or intentional powder oxidation was conducted to simulate the powder degradation over a period [5,7]. However, there is still a lack of systematic approach to assess the powder degradation in LB-PBF using appropriate surface analysis tools over a prolonged reuse of powder.

In the current study, the powder degradation analysis has been conducted on AlSi10Mg powder which was reused over the period of 30 months in the XLINE 2000R LB-PBF machine (Concept Laser GmbH, GE Additive company). The powder particles oxidation (powder surface oxide morphology, characteristics of surface oxide, etc.) has been investigated over regular intervals based on the machine running time. The volume fraction of spatter particles in the powder bed has been evaluated and detailed analysis of the powder surface chemistry and its changes with powder reuse time has been performed by means of surface sensitive techniques as X-ray photoelectron spectroscopy. Oxide cross-section on the powder surface was further studied by scanning transmission electron spectroscopy. Furthermore, a comparative analysis has been done between the powder and spatter particles, and the variation in surface degradation mechanism have been examined. The experimental findings has been further investigated in retrospective of thermodynamic calculations using Thermo-Calc [23] and HSC Chemistry. Finally, the possible impact of powder oxidation and spatter concentration on the built component properties has been discussed.

2. Materials and methods

Aluminum alloy powder with the nominal composition Si 10.1 wt.%, Mg 0.4 wt.% and Fe 0.11 wt.%, rest Al, provided by Concept Laser GmbH, was studied. Powder has a particle size distribution with D10= 45 μm, D50=65 μm and D90=93 μm, measured using laser diffraction particle size analyzers utilizing Mastersizer 3000, Malvern Panalytical, UK. The powder was produced via nitrogen gas atomization, resulting in nearly spherical powder particles with the presence of some satellites, meaning fine particles smaller than 5 μm which can adhere to bigger particles.

The powder is processed with a metal laser powder bed fusion machine XLINE 2000R with the build envelope 800 x 400 x 500 mm^3. Recycling and storage of the powder take place in a separated sieving station and silo. Both, silo and sieve are interconnected and linked to the LB-PBF machine with pipelines. The closed system is permanently flooded with fresh nitrogen (maintaining oxygen content around 0.1 %) for the prevention of powder oxidation. However, at the end of the process, the build plate with the additively manufactured components, which are surrounded by non-molten powder, is moved from processing station into the glove box for further operations. During this process, build chamber and un-used powder is exposed to the ambient air environment for a few minutes. Further on, un-used powder is extracted from the build volume in the closed and inert atmosphere of the glove box. Powder is transported automatically by inert gas through pipelines to the sieving station in which particles bigger than 100 μm in diameter are sieved out.

The system is operating with approximately 550 kg of AlSi10Mg powder at any time. The loss of powder due to the manufacturing of components is compensated by adding a certain amount of virgin

powder. In summary, the powder mixture used for the investigation consists of virgin and reused powder. The reused powder, studied in this work, is the result from continuous utilization of the LB-PBF machine over 30 months with a system operation of approx. 2000 h each year. Overall, five samples were collected over the period of 30 months to examine the change in powder quality and hence degradation rate. Table 1 is showing the time frame and annotation for each sample used in this study.

Surface chemistry of the powder and its changes during powder use in terms of the oxide layer thickness, composition and chemical depth profile, was studied using X-ray Photoelectron Spectroscopy (XPS) utilizing PHI 5500 (Physical electronics, MN, USA) equipped with a monochromator Al Kα source (1486.6 eV). Considering the low hardness of the powder, powder samples were prepared by light pressing of the powder into indium plate to avoid the damage on the powder surface. To get the depth profile, etching was conducted using Ar+ ion gun where the etch rate was calibrated using Ta_2O_5 with known oxide layer thickness and hence etch depth and oxide thickness are presented in Ta_2O_5 units. The data obtained from XPS were further analyzed using PHI Multipak software. The normalized oxygen content profile with the etch depth and oxide layer thickness was calculated by using O1s and Al2p peaks, respectively. In normalized oxygen content calculation, peak area of O1s peak was normalized to establish a comparative analysis of the oxygen profile change, indicating in-depth distribution of the oxide phases between the samples. To attain the statistical authenticity, all the XPS measurements were repeated 3-4 times.

For surface morphology and topographical analysis, scanning electron microscopy (Leo Gemini 1550 SEM, Zeiss Gmbh) equipped with field emission gun and In-lens detector was used. The In-lens detector was used to obtain good resolution at higher magnification. Transmission electron microscopy (TEM), namely a FEI Titan (FEI/ Thermo Fisher Scientific, UK) equipped with Silicon drift (SSD) EDX detector (Oxford Instruments, UK), was used to investigate the microstructure and oxide scale on the spatter particles. For the purpose of oxide morphology and composition analysis on a powder cross-section, TITAN was operated in scanning transmission electron microscope (STEM) mode at 300 keV and sample was titled at 15° towards the detector for EDX data acquisition. A typical TEM sample of an average thickness of 100 nm was prepared using FEI Versa 3D focused ion beam (FIB) milling system.

Spatter particles distribution was calculated by using the low magnification images from SEM and employing ImageJ software. Overall, 10 images per sample were examined to get a mean percentage of the spatter particles in the powder bed. The oxygen content was measured using Horiba oxygen and nitrogen analyser EMGA-620 W (Horiba Scientific).

3. Results and discussion

3.1. Bulk powder analysis

Gradual coarsening of powder during LB-PBF has been observed in several alloys after multiple reusability cycles [16,17,24]. Therefore, sieving is an essential process in the PBF techniques as it helps to maintain the consistent size distribution. This is done in order to assure build parts reproducibility and process stability through removal of agglomerated particles to assure consistent rheological properties of the powder and packing density. Getting rid of particles smaller than D10 to avoid airborne particles and dusting is trickier and is not typically performed during sieving of reused powder and hence fine spatter is staying in the powder bed. Furthermore, it is a general expectation that the unwanted spatter particles generated in previous build, coarser than 100 μm, can be sieved out to avoid any defects in the future builds. Fig. 1 is illustrating a comparison of powder particle size distribution (PSD) between virgin and recycled powder. In both cases, PSD lies in the range of 40 μm to 100 μm with D10= 45 μm, D50=65 μm and D90=93 μm. Although it is not significant, the curve representing Al30 is showing a slight shift towards smaller particle size distribution as compared to Al0 where D10=44 μm, D50=64 μm, and D90=90 μm. This suggests that the agglomerated particles were successfully removed during sieving process. On the other hand, the value of D10 is consistent over time which assumed to be linked with the removal of agglomerates from one side and removal of fines by the processing atmosphere during the process and adherence of fine particles during transportation to the surfaces of the powder supply system components. The consistency of particles size distribution redundant the possibility of defect formation by aforementioned factors as well as removes the agglomerated spatter particles. The latter claim will be further examined in the following results where the presence of spatters with similar size distribution as powder will be analyzed.

To estimate the variation in oxygen content over time, a comparative analysis of bulk oxygen content in the powder is shown in Fig. 2 where an incrementing tendency in oxygen content increasing was observed with reuse time of the powder. The oxygen content has shown a sharp increase from Al0 to Al6 due to the increase in the thickness of the initial oxide layer due to the handling of the powder. However, the rate of oxygen content increase slows down after 6 month due to the powder surface passivation connected to the formation of stable Al-oxide layer.

3.2. Microstructural analysis

To evaluate the morphology of the powders, low magnification imaging was conducted as displayed in Fig. 3. The difference between powder shape and size distribution in both samples is insignificant except the presence of some satellites in Al0 powder. However, some “bright” particles can be clearly seen in the Al30 which were not present in the Al0 powder. The “bright” appearance of the powder particles is due to the lower conductivity of the specific powder particles in

Table 1
The annotation of the samples with respective time in the LB-PBF XLINE 2000R machine.

Sample name	Time in machine
Al0	Virgin powder
Al6	6 months
Al10	10 months
Al14	14 months
Al30	30 months

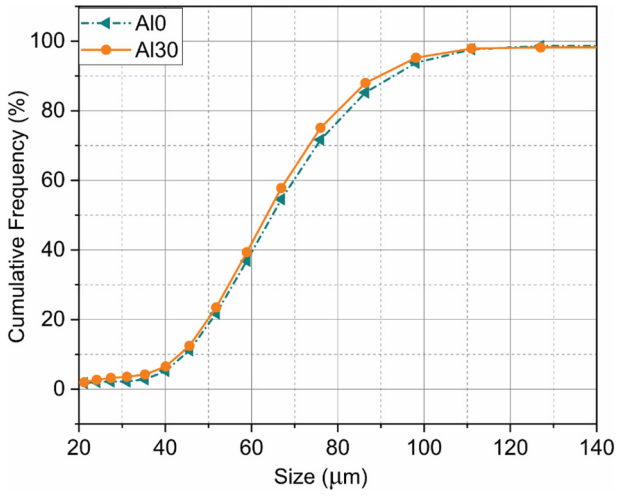

Fig. 1. Comparison of the powder particles size distribution in Al0 and Al30 powders.

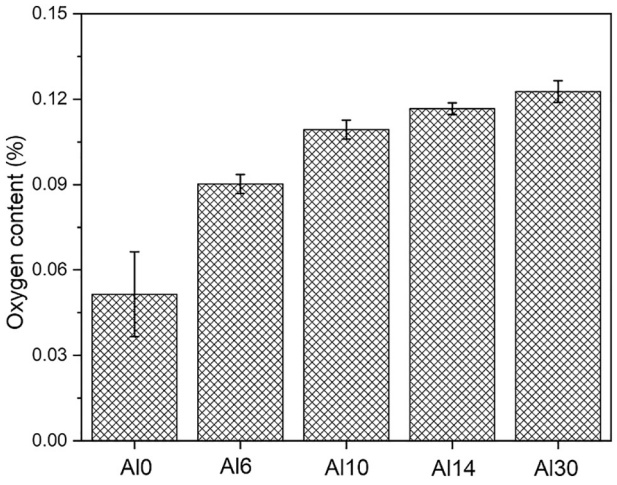

Fig. 2. Oxygen content analysis of all the samples from Al0 to Al30.

comparison to other particles, that is the indication of powder oxidation and hence is a hint that these particles are spatters generated during the fabrication process [18,25,26]. Observed spatter particles are also characterized by spherical shape. To highlight the presence of spatter particles in the samples of powder after reuse and show the incrementing tendency in the volume fraction, a comparison of the powder is shown in figure S1 (supplementary data). Spatter particles in Al6 sample were in trace amount whereas sputter particles were more clearly observed in powder with increasing reuse time.

To effectively investigate the degradation of the powder over the period of thirty months, the morphology of the powder particles from Al0 (fresh) and Al30 (reused for 30 months) was analyzed. Fig. 4 is showing a comparison between the Al0 and Al30 to show the variation in the surface morphology of the powders. Several micron-sized satellite particles are attached on the surface of Al0, however, the surface of the reused powder in Al30 is much smoother with the absence of any satellite particles as a result of the multiply sieving during powder reuse and friction between particles during transportation in the AM machine (pipelines, etc.) and hence satellite removal. Presence of fine satellite particles in case of virgin powder can be clearly seen in Fig. 4a. However, there were no any secondary phases observed on the powder surface after reuse as is typically done in case of reused powder in case of Fe- and Ni-base materials [14,18,26].This is due to the fact that the matrix element – aluminum – has the highest thermodynamic stability of oxide after magnesium and hence resulting in a formation of a stable Al_2O_3 and/or Al-Mg-oxide (e.g. $MgAl_2O_4$) layer.

The microscopic analysis of bright/oxidized particles observed in the reused powder, shown in Fig. 3, was further evaluated at higher magnification and compared with powder particles in the same powder but not possessing any contrast differences, e.g. representing the bulk of the powder samples. Fig. 5a is showing the surface morphology of the unaffected powder particle with a smooth surface and absence of any oxide particulates. Contrarily, spatter particle is showing a presence of

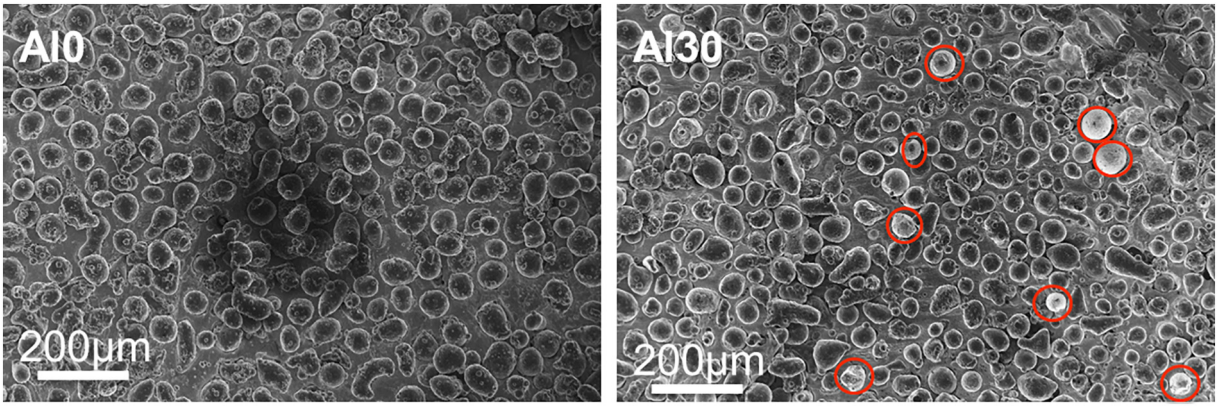

Fig. 3. Low magnification imaging of Al0 and Al30 where the red circles in the Al30 image are highlighting the bright oxidized particles present in the reused powder. (For interpretation of the references to color in this figure legend, the reader is referred to the web version of this article.)

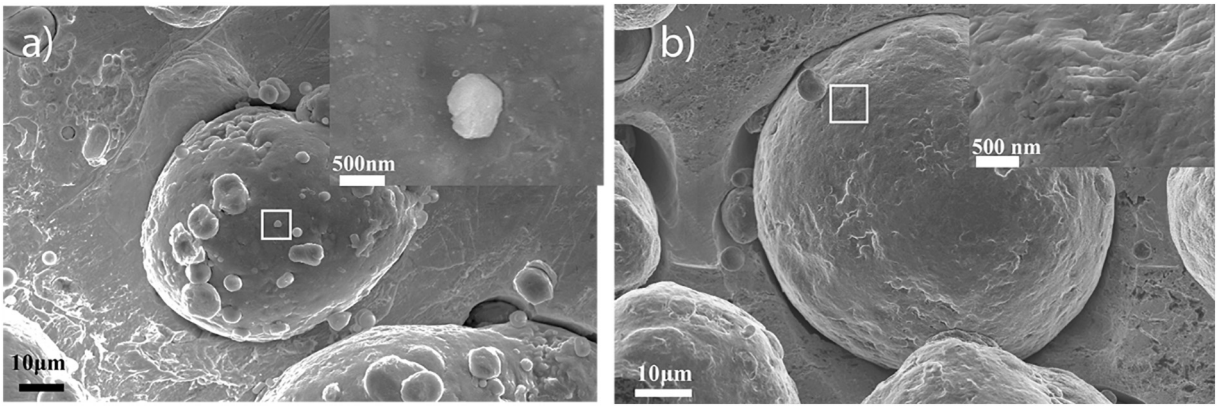

Fig. 4. Comparison of surface morphology at lower and higher magnification (insert) of particles from a) Al0 and b) Al30.

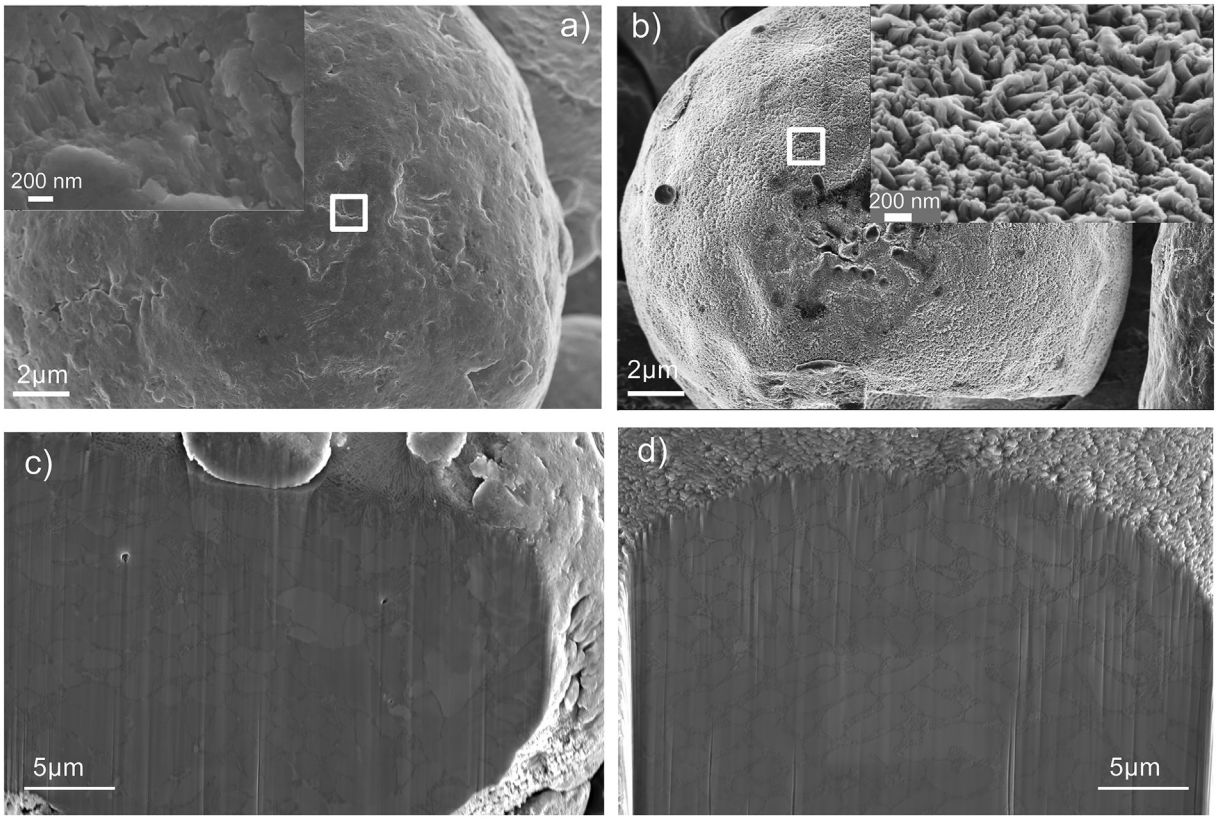

Fig. 5. Surface morphology and FIB cross-section of a, c) representative powder and b, d) spatter particles in Al30 sample.

morphologically rough surface of the powder particle [25]. Such surface texture hasn't been observed in the virgin powder at all. This clearly show changes in the physical properties and chemical composition of the powder surface, assuming that powder was oxidized during LB-PBF processing due to the interaction with the processing atmosphere. The well-defined spherical shape of the spatters is an indication of full solidification before particle landed in the powder bed, allowing molted particle to take spherical shape to minimize the surface energy. Due to the high affinity of Al to oxygen, it is neither possible nor technically feasible to reach such oxygen potential in the processing atmosphere (partial pressure of oxygen) required to avoid oxidation, especially in powder form [27]. Hence, oxygen potential in the system is always high enough to promote oxidation. Local availability of the oxygen during spatter solidification along the spatter track, that is proportional to the oxygen content above the powder bed, determines kinetics of the surface oxide growth. In order to confirm formation of the oxide layer on the spatter particles, analysis of the powder cross-section was conducted by FIB, see Fig. 5 (c, d). There is a clear indication of the presence of the coarse surface oxide layer in case of the sputter particles, see Fig. 5d. The microstructure observation of the powder particles shows that the grain structure also is very different between virgin and spatter particles. In case of spatter particles, grains were homogeneously equiaxed as compared to the dendritic structure of the unaffected particles, probably due to recrystallization or more rapid solidification, depending on the spatter particle origin, temperature and size.

The quantification of the sputter particle content obtained by means of the image analysis and surface morphology of the spatter particles in case of Al10, Al14, and Al30, is presented in Fig. 6. The graph in Fig. 6a is illustrating the percentage of spatter particles which is calculated through the series of image analyses. From each sample around ten low magnification images were taken with controlled brightness and contrast. Furthermore, the spatter particles were individually confirmed by investigating the morphology at higher magnification. After rigorous analysis and counting more than ten thousand particles, this graph was plotted with appropriate error bars based on the standard deviations. The graph shows the absence of oxidized particles in the virgin powder sample Al0, confirming the assumption that observed heavily oxidized powder particles are sputter. Insignificant percentage of sputter particles was detected in Al6 powder. However, there exist an increasing trend from Al10 to Al30 where the percentage of spatter particles in Al10 is just below 1% (0.78%) and 1.23% in Al14. The fraction of sputter particles substantially increases to a value of 3.15% in case of Al30 powder. Hence, it can be concluded that there is a proportional relationship between the percentage of spatter particles and the time in the machine. The amount of oxide particles is quite significant considering the thick columnar scale which probably is oxide and can result in various type of defects as e.g. oxide accumulation, porosity formation, etc. The Fig. 6b is showing a comparison between the morphology of the spatter particles from Al10, Al14, and Al30. The surface morphology of the powder surface oxide looks similar which reaffirms the unanimity of formation process.

To establish an understanding about the nature of nodules and oxide layer thickness on spatter surface, energy dispersive X-ray spectroscopy (EDX) was performed using transmission electron microscopy (Titan) in STEM mode. The Fig. 7a is showing a FIB cross-section where nodules height and morphology can be observed. The nodules are randomly oriented on spatter surface and form fine dendritic pattern. Oxide layer, formed by nodules, is not homogeneous in thickness where high roughness of surface oxide is observed, with nodules often penetrating deeper into powder particle surface (see yellow arrow on Fig. 6). This interesting trend is visible in the TEM sample shown in Fig. 7b. Before the sample preparation using FIB milling, the surface was covered first with thin protective layer of electron beam assisted platinum (Pt) layer and then

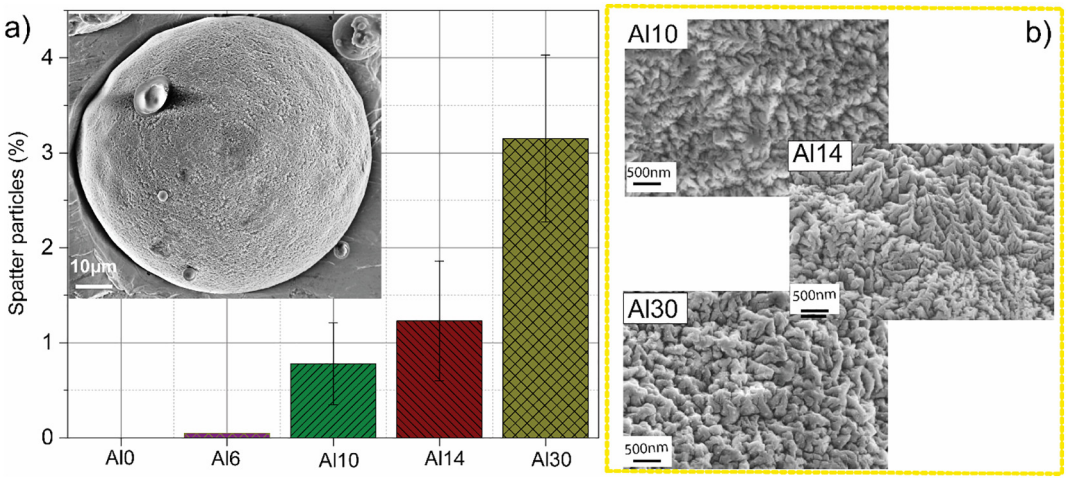

Fig. 6. a) The quantification of spatter particles in all the samples and b) comparison of the surface morphology of spatter particles in case of Al10, Al14 and Al30.

subsequently deposited Ga^{+} assisted Pt layer. The height of nodules from the surface of the sample lies in the range of 50-125 nm. Interestingly, there was no uniform oxide layer formation observed on the spatter powder particles. This can be attributed to the extremely short time-frame spatter had to fly from the melt pool and its surroundings and solidify in a rather controlled environment. During the oxidation process, formation of nodules is an initial nucleation stage of oxidation which has been observed on the spatter particles. Non-uniform oxide growth is attributed to a very short time at high temperature, controlled environment meaning limited supply of the oxygen and potentially full or partial melting of the particle.

To estimate composition of the oxide scale observed, a STEM-EDX line scan was acquired near the spatter surface over the nodules and results are shown in Fig. 8. The concentration profiles of Al and O are showing their consistent presence throughout the line scan indicating presence of Al-based oxide, i.e. Al_2O_3 which is the most stable oxide in the system after MgO. The Si content indicate absence of Si in the surface oxide scale and presence of Si-rich phase just below the oxide layer, probably silicides of Fe and Al, as enrichment in iron was observed just underneath of oxide layer, even though closer to the interface than Si. Moreover, a small peak of Mg appeared near the top surface distinct from Al peak on EDX scan. After 100 nm depth, the Mg content was merely a background noise. Hence, a small Mg concentration exist in top oxide layer probably in the form of $MgAl_2O_4$ spinel present in nodular α-Al_2O_3 oxide scale. Thickness of nodule in the current scan is around 85 nm, but it varies from 50-125 nm.

3.3. XPS analysis

Chemical composition and thickness of oxide layer is considered essential to understand the degradation mechanism of powder during AM processing, and XPS is potentially the best tool to serve this purpose [28–32]. The survey spectra of all samples are compared at as received and 4 nm etched surface to evaluate the chemical composition of the powder surface. Fig. 9a shows survey spectra of all powders in as-received state where peaks of Al and Mg can be observed along with C1s, In3d and O1s peaks. The In3d peak is originated from the foil used for powder mounting while C1s is showing the absorbed carbon species on as received surface. The Si peak on as received surface appeared with a very low intensity indicating the absence of Si in surface oxide, in agreement with STEM+EDX results. Interestingly, Mg1s peak was not observed on the surface of virgin powder (Al0 sample), whereas Mg1s peak intensity significantly increased with powder aging, reaching surface concentration close to aluminum in case of Al30 powder. This signifies the development and growth of the oxide layer proportional to the aging time, e.g. based on the increased number of sputter particles and hence higher contribution to the measured surface composition. It is important to remember that 200 µm×200 µm area is analyzed during XPS analysis and hence provides general overview of the powder surface chemistry, including contribution from the surface oxide by spatter particles.

The high-resolution spectra over the binding energy of Al2p, Mg1s and O1s were measured to further evaluate the oxide type and its

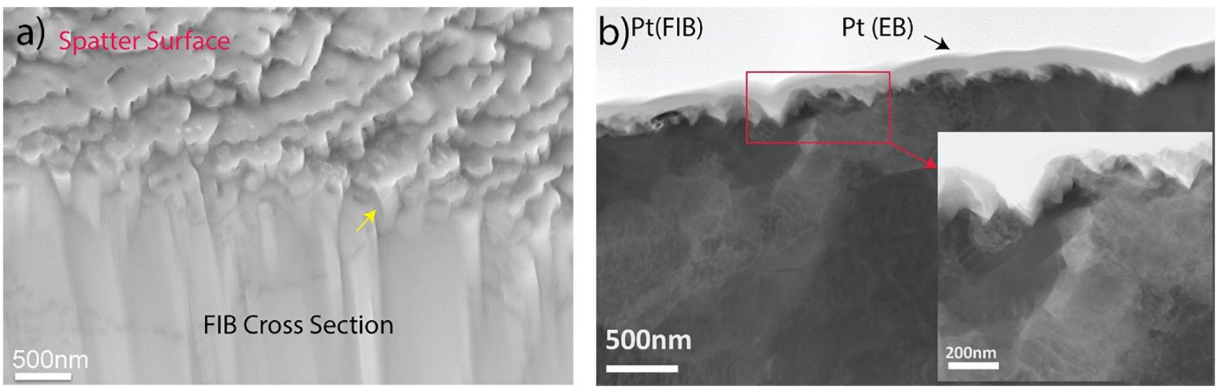

Fig. 7. a) FIB milled cross-section and b) high angle annular dark field (HAADF) image of spatter particle of Al30.

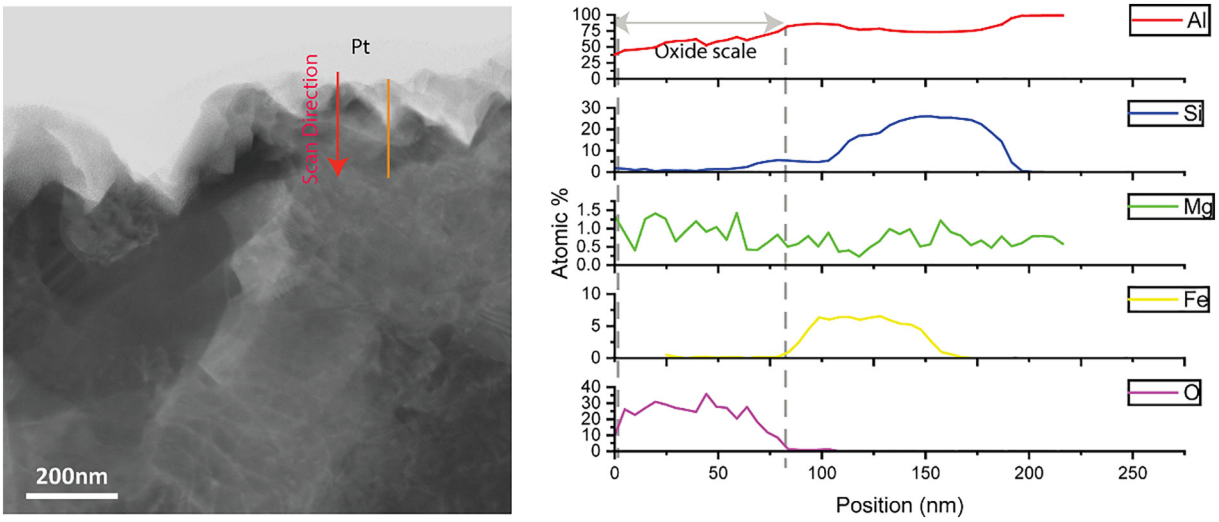

Fig. 8. The EDS line scan on oxide nodules in spatter particle of Al30.

distribution on the powder surface. The results are illustrated in Fig. 10 where shift parameters were adjusted by using Al^0 peak at 72 eV as measured on pure Al-standard. The corresponding standard peak positions were obtained from XPS analysis of pure Al plate and $MgAl_2O_4$ standard powder sample and values are summarized in Table 2. From Al spectra shown in Fig. 10, a relatively high intensity of Al^0 can be observed along with Al^{+3} which indicates that the thickness (t) of oxide layer is lower than 3λ (the attenuation length of photoelectrons for Al_2O_3 ~2 nm). Thus, the thickness of oxide layer in a virgin powder is in few nm ranges. Whereas, the intensity of Al^0 gradually decreases with powder aging, see e.g. sample Al10 (Fig. 10b) and almost fully disappeared in Al30 (Fig. 10c), which is highlighting the increase in Al-based oxide layer thickness in general during powder handling for such a long time.

A similar trend exists in Mg spectra where Mg^{+2} was not observed in Al0 powder, indicating rapid powder solidification during atomization, allowing to avoid Mg-segregation to the powder surfaces and its further oxidation. Hence, surface of the virgin powder is covered primary by Al-rich oxide. However, Mg1s peak appeared in Al10 and Al30 samples. Additionally, the intensity of Mg^{+2} peak in Al30 is substantially higher than in Al10. Hence, the persistent presence of Mg^{+2} peak in recycled powders represents a significant enrichment of Mg^{+2} at the top layer of surface oxide, either as rock-salt type MgO or as a spinel-type $MgAl_2O_4$. At the same time, the intensity of Al^{3+} peak is consistent from as received to etched surface indicating the presence of thick α-Al_2O_3. This assumes increasing amount of $MgAl_2O_4$ spinel on the top surface of the powder oxide layer from Al0 to Al30 with the ageing of the powder. Presence of the $MgAl_2O_4$ spinel oxide was confirmed by Al^{3+} and Mg^{2+} peak positions, obtained using a $MgAl_2O_4$ standard. This agrees with the EDS analysis during STEM, where enrichment in Mg oxide in the nodules on the spatter particles was clearly shown, see Fig. 8. Hence, it is believed that the increase in the intensity of Mg^{+2} might have been connected to the enrichment in Mg in oxide formed on spatter particles rather than its enrichment on the reused powder due to the long-term powder handling (e.g. long-term exposure to the processing gas without exposure to the laser during processing).

Moreover, a shift can be observed in all three spectra from as received surface to 1 nm etched depth. This shift is more prominent in reused powder by the appearance of Mg^{+2} peak. This shift is suggesting the presence of both, Mg^{+2} and Al^{+3} in the form of hydroxides. By peak

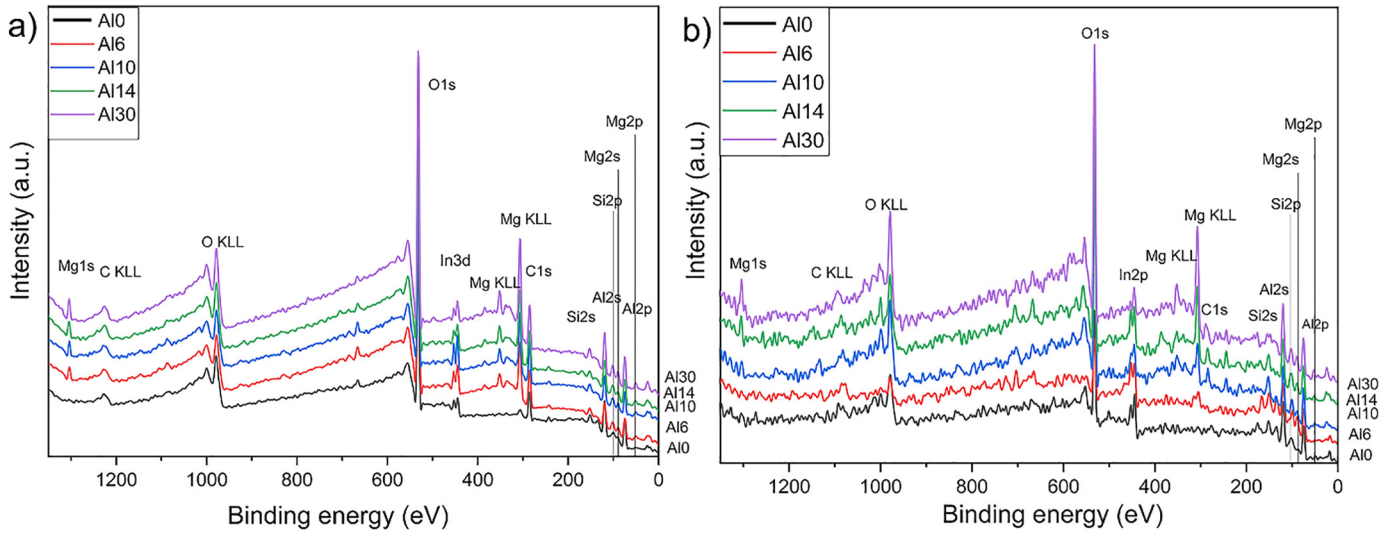

Fig. 9. XPS survey spectra at a) as received surface and b) etch depth of 4nm

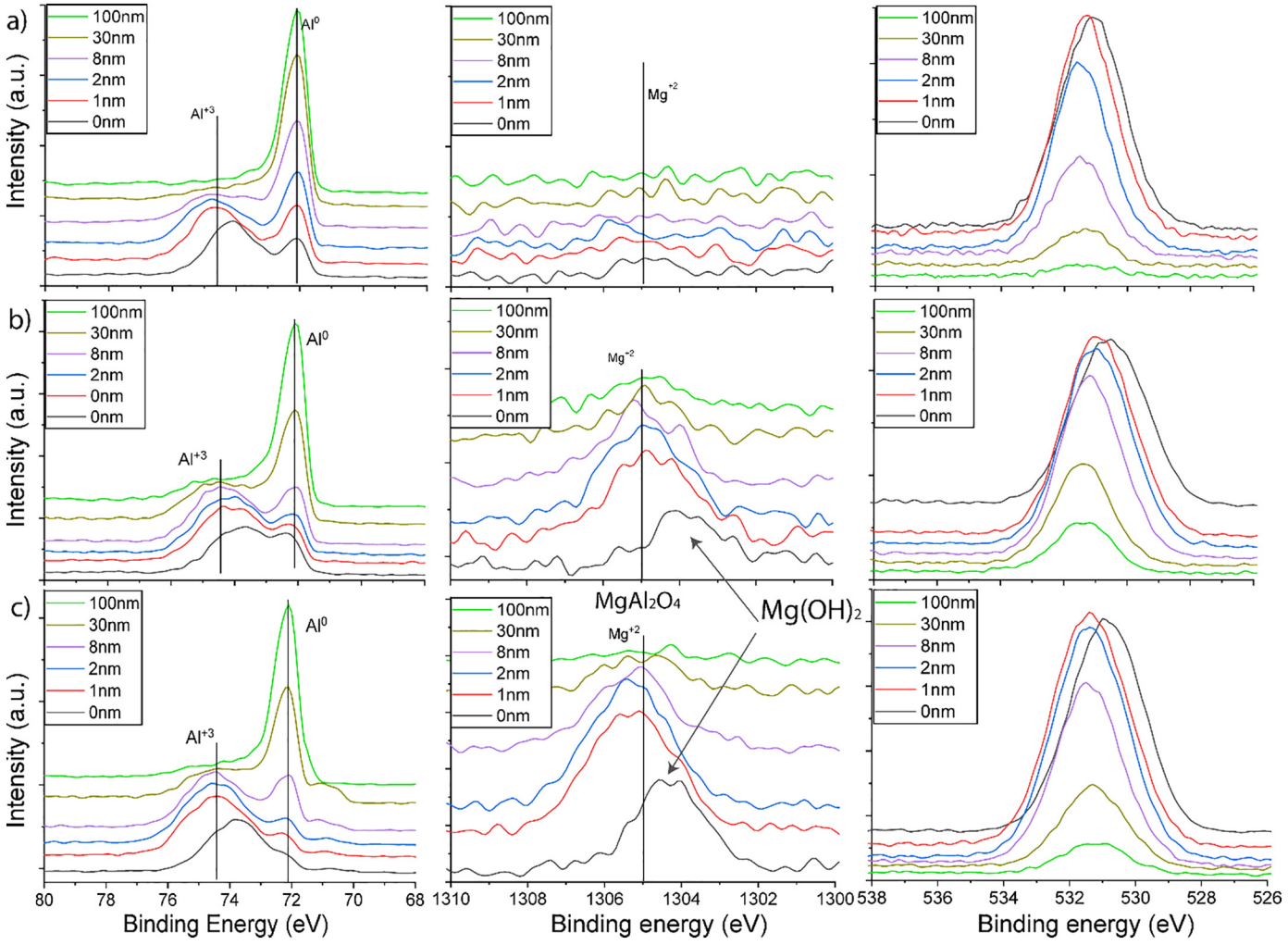

Fig. 10. The XPS narrow scans over the binding energy of Al2p, Mg1s and O1s and depth profile of a) Al0, b) Al10 and c) Al30 powders.

deconvolution, it is estimated that Mg^{+2} is forming halite and Al^{+3} is forming gibbsite type of hydroxide.

The analysis of oxygen peak O1s intensity change throughout the etch depth shows a comparable trend in all samples, see Fig. 11a, where peak broadening was observed with powder aging time. The broadening of the peak is an indication of the change in composition and thickness of the oxide layer, covering powder surface [30]. It is important to note that around 20 particles are analyzed during XPS analysis, meaning that oxygen profile represents both, reused powder as well as spatter particles, present in the reused powder. As spatter particles are covered by rather thick oxide layer up to 120 nm thick, and concentration of such particles is increasing with powder reuse, see Fig. 6, this will result in the broadening of the oxygen profile. Therefore, the oxygen content profile illustrated here is a mean of powder and spatter particles, determined by their concentration in the reused powder.

Similarly, the oxide layer thickness illustrated in Fig. 11b is showing an evolution in average oxide layer thickness with ageing. The oxide layer thickness was measured using the aluminum metal peak Al^0 intensities at different etch depths normalized to the intensity at final etch depth (where Al^{3+} peak disappears) using $I_0/I_{0\text{-}100}$ (I_0 is the intensity at any given depth and $I_{0\text{-}100}$ is corresponding to the intensity where 100% metallic peak appear in spectra) [31]. Considering the layer thickness and mean free path (λ, which is 2 nm for Al_2O_3 [36]), the etch depth giving a normalized intensity value at 66% was taken as the oxide layer thickness as suggested by Oikonomou et al. [31]. As discussed previously, the presence of the metal peak in Al0 sample even on the as-received surface (before Ar+ etching) indicate presence of thin oxide layer, formed by Al_2O_3, with the thickness of around 4nm. Nonetheless, there is a substantial growth of oxide layer to 18 nm already after 6 month of powder reuse, which explains the sharp increment in oxygen content presented in Fig. 2. The oxide thickness

Table 2
XPS binding energies of reference and fitted Al30 powder sample in eV, peak position is corrected using $Al^{met}2p$ at 72 eV.

	Peak position (eV)	FWHM	Ref
Al^0 (Al-plate)	72	0.5	
Al^{3+} (Al_2O_3)	74.75	1.27	
Al^{3+} ($MgAl_2O_4$)	75.42	2.07	
Al^{3+}(AlOOH)	73.63	1.58	[33]
Mg^{2+}($MgAl_2O_4$)	1304.9	1.52	
Mg^{2+}($Mg(OH)_2$)	1303.9		[34]
O^{2-} (Al_2O_3)	531.71	2.07	
O^{2-} ($MgAl_2O_4$)	531.80	2.55	
O^{2-} (MgO)	530.5		[35]
C1s	285	1.82	

*A pure Al plate (99.99 %) was cleaned by ion etching in XPS chamber to get rid of oxides and carbonaceous impurities; then plate was removed from XPS chamber for couple of minutes to develop an oxide layer. Sample was reintroduced in XPS for standard measurements reported here.

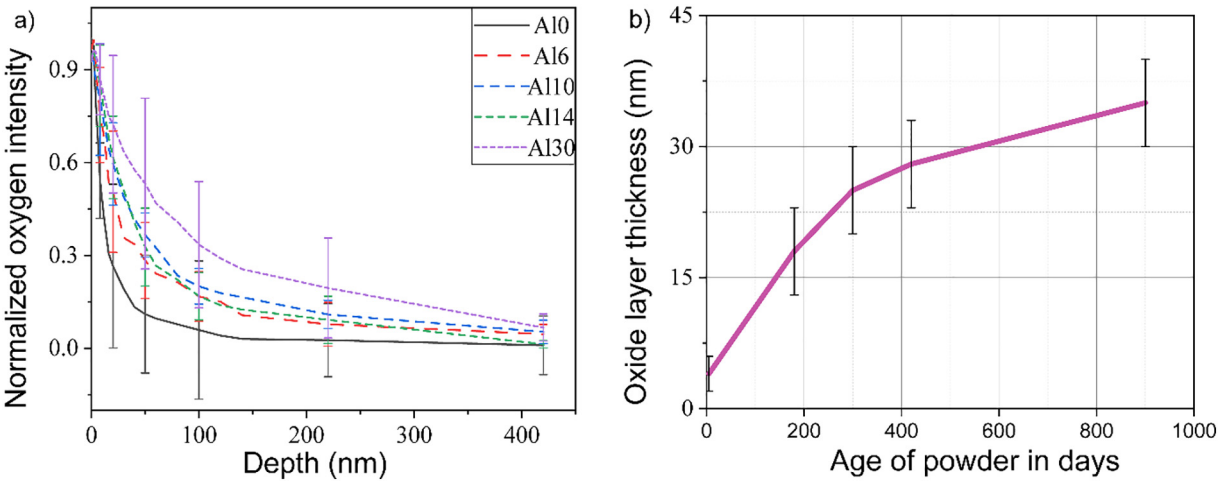

Fig. 11. A comparison of a) normalized oxygen intensity with the etch depth and b) average oxide layer thickness of Al0, Al6, Al10, Al14, and Al30.

continuously increased with ageing of the powder and the thickness of about 38 nm was registered in case of Al30 samples. Again, the oxide thickness value here is the mean value, representing contribution from the aged powder particles as well as spatter particles, corresponding to their fraction in the powder, as in in Fig. 6a, where e.g. around 3 % spatter particles are present in the Al30 samples. Hence, the value of the ~38 nm is not representing the oxide thickness in case of spatter particles as it is significantly larger, as indicated in Fig. 8. Even though sputter generation is continuous process and hence linear increase in average oxide layer thickness could be expected if solely based on the sputter accumulation with time, non-linearity of the evolution of oxide layer thickness with time is evident. As-manufactured powder is typically packed under protective gas and is characterized by the low oxygen content, reflecting low thickness of surface oxide. Hence, initial increase in oxide layer thickness is believed to be connected to the initial oxygen pick-up by the virgin powder during powder loading and processing of the powder (LPBF process and further powder sieving), exposing it to the air and oxygen-rich atmosphere, leading to initial growth of the surface oxide layer thickness to the equilibrium value for the powder, that is further stabilized and is stable with time, as was shown in case of Ti- and its alloys [37]. Further increase in the average thickness of the surface oxide is connected to the accumulation of the spatter particles, where linear increase is assumed. However, as virgin powder is added cyclically to compensate the used amount during the fabrication process, this will further affect the average oxide layer thickness and deviation from the linear trend. The similar trend can be observed in variation in oxygen content over time given in Fig. 2, which reaffirms the non-linear tendency of growth in oxide layer thickness. Similar non-linear increase in oxygen pick-up was observed during powder degradation in EBM process [7,18].

3.4. Thermodynamic calculations and analysis

AlSi10Mg alloy contains active elements with higher susceptibility to oxygen. Microstructural and XPS analysis have showed formation and growth of oxides on AlSi10Mg powder surface by aging over the period of 30 months. Therefore, thermodynamic calculations have been conducted to confirm the experimental findings. Fig. 12 is showing a comparison of change in Gibbs free energy (ΔG) of SiO_2, Al_2O_3, MgO and $MgAl_2O_4$ over a range of temperature using Ellingham diagram (Fig. 12a), and relative stability of these oxides with varying oxygen partial pressure and temperature (Fig. 12b). Both ΔG and stability of oxides are following the same trend where the oxide stability is increasing as follows: $SiO_2 < Al_2O_3 < MgAl_2O_4 < MgO$.

The above calculations are true for oxides forming from pure elements and gives valuable information on their relative stability. However, the oxides on the sputtered particles are formed from a liquid with a composition of Al, Si 10.1 wt.%, Mg 0.4 wt.% and Fe 0.11 wt.%.

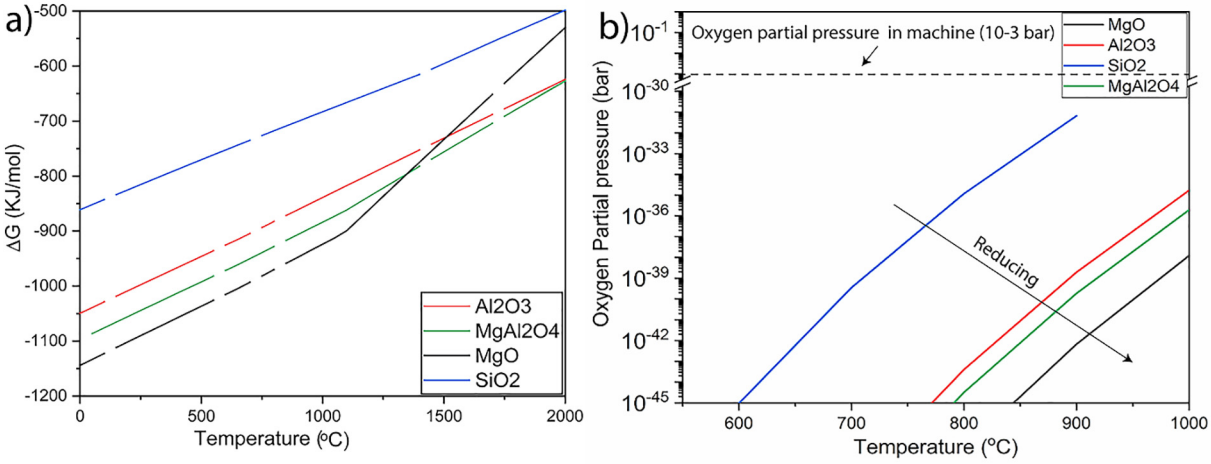

Fig. 12. Stability of various oxides potentially present in the system using Ellingham diagram and oxygen partial pressure.

The CALPHAD method [38] is a well-established technique for assessment and calculation of thermo chemical information and phase equilibria for multi component systems. In present study we have used Thermo-Calc, that is a powerful software package for the calculation of thermodynamic and phase equilibria for multicomponent systems. In conjunction with suitable thermodynamic databases, assessed using the CALPHAD approach, Thermo-Calc can be used for a wide variety of applications. In Fig. 13a, the equilibrium phase fractions for the liquid sputter particle at different partial pressures of O_2 is shown, calculated with Thermo-Calc using TCOX10 [23] database. The calculation is performed at 1000 °C, well above the melting temperature for the alloy (~600 °C). At very low partial pressures of O_2 only the liquid is stable but at increasing partial pressures Al_2O_3 (Corundum), $MgAl_2O_4$ (Spinel) and SiO_2 (Tridymite) are stable if equilibrium is reached. Note that MgO is not predicted to be stable. Since spattered particles exist in liquid state, where most of oxides are formed, only for a very short time, it can be assumed that equilibrium is not reached and that the oxides with highest driving force for precipitation are formed first.

In Fig. 13b the driving force (ΔG) for the different oxides forming from the liquid with Al, Si 10.1 wt.%, Mg 0.4 wt.% and Fe 0.11 wt.% is calculated at partial pressure 10^{-4} O_2 (bar) with Thermo-Calc using TCOX10 [23] database. The calculation shows that only Al_2O_3 (Corundum) and $MgAl_2O_4$ (Spinel) can form directly from the liquid (ΔG is negative) at all temperatures. SiO_2 (Quartz, Tridymite, Cristobalite) and MgO have a positive ΔG meaning they will not form directly from the liquid at any temperature. Note, SiO_2 will have negative ΔG once Al_2O_3 and $MgAl_2O_4$ have formed in large amount and depleted the liquid from Al and Mg. However, since Al_2O_3 and $MgAl_2O_4$ are seen to form a continuous shell at the surface of sputtered particles and protect the remaining liquid from oxidation, this depletion will never happen and SiO_2 will remain unstable.

Powder degradation was an expected consequence from a prolonged (about 5000 h over the period of 30 months) powder reusage. The results have assisted in establishing an understanding of dominant powder degradation mechanism among homogeneous powder oxidation and spatter formation. Due to the nature of the oxide in Al-based alloys, powder degradation result in continuous increase in oxide layer thickness instead of formation and growth of particulate oxide features, as in case of Fe-and Ni-base alloys [14,18,32]. The spatter particles presence and their respective fraction in reused powder raised the alarm about extent of powder degradation and appeared as the dominant degradation mechanism. The quantification of the spatter particles has shown a significant increase in the volume fraction of spatter particles up to 3% after reuse for 30 months. Interestingly, the surface of spatter particles showed the formation of oxide scale with irregular morphology giving an evidence of surface oxidation during melting and solidification of spatter particle. In an oxidation analysis of alumina-forming PM2000 Fe-alloy, Djebaili et al. [39] observed the formation of interconnected scales of α-Al_2O_3 with incorporated cracks and porosities at 1473K. Although those observations were for bulk sample and long-time exposure, the mechanism provides an insight regarding formation of such nodular structure of oxide scale on spatter particles. STEM results helped to verify the presence of oxide scales, containing mainly Al and Mg, varied in thickness from 50 nm to 125 nm. To further evaluate the influence of powder reuse and spatter presence on the level of oxidation of the powder/sputter surface, XPS analysis was used. The XPS analysis showed an increase in oxide layer thickness, from ~ 4 nm in case of virgin powder to about 38 nm after powder reuse for 30 months, indicating powder degradation proportional to time of reusage. XPS was further used to understand the presence of Mg in oxide layer which happened to form $MgAl_2O_4$ spinel oxide in Al_2O_3. Thermodynamic calculations conducted on the condition of spatter particle before solidification have reaffirmed the experimental findings where $MgAl_2O_4$ and Al_2O_3 directly formed from the liquid form. Formation of $MgAl_2O_4$ and Al_2O_3 on top surface hindered further oxidation of Si. In addition, presence of Al- and Mg-hydroxides on the top powder surface was detected by XPS in case of all powders, with increasing content in case of reused powders. Hydroxides formation is believed to be connected to the general powder handling for such a long period of time, where it is periodically exposed to the ambient air as well as residual humidity from the processing gas. Hence, slight increase in hydroxide content in the powder is believed to be connected to all particles and not specifically to sputter particles, as in case of e.g. $MgAl_2O_4$ spinel formation and Al_2O_3 oxide layer growth.

Overall, the results showed increase in both, bulk oxygen content and oxide layer thickness. This increase in oxide layer thickness brings a significant risk in the oxide accumulation during the melting and increase in defect formation. The phenomenon of oxide accumulation has been discussed by Gruber et al. where the oxide layer doesn't dissolve in the melt pool and stay on top of the melt pool and form oxide defects in the fabricated part [22,40] seriously harming the resultant mechanical properties of the product. With formation of oxide layer

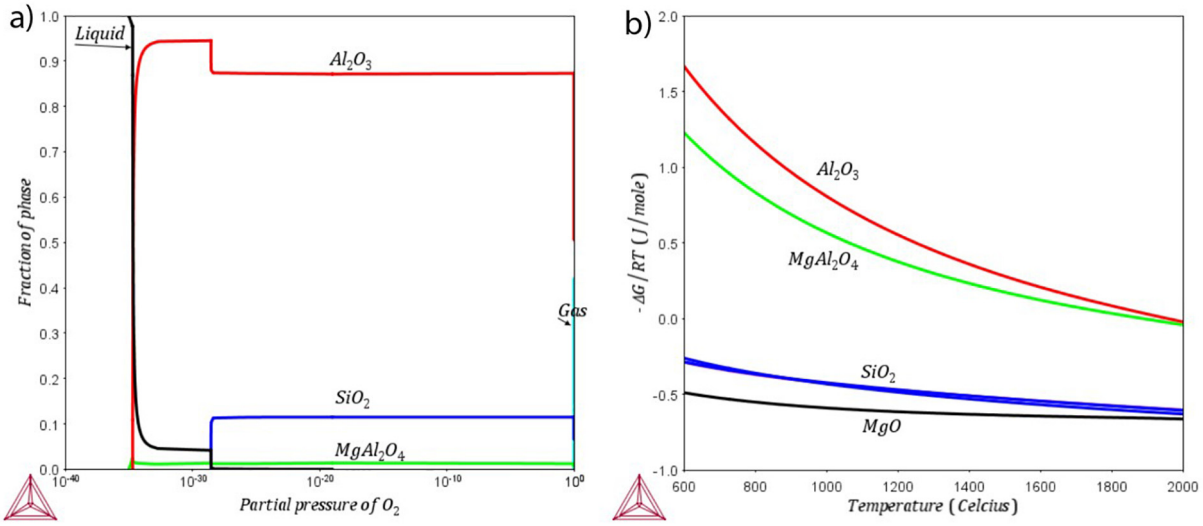

Fig. 13. Thermodynamic calculations using Thermo-Calc: a) Equilibrium phase fractions for the liquid sputter particle at different partial pressures of O_2, calculated at 1000 °C with Thermo-Calc using TCOX10 database and b) Driving force (ΔG) for the different oxides from a liquid with Al, Si 10.1 wt.%, Mg 0.4 wt.% and Fe 0.11 wt.%, calculated with Thermo-Calc using TCOX10 database.

on top of the melt pool, an additional factor related to change in surface tension can come in play which can change the direction of melt from centrifugal to centripetal flow by changing the Marangoni effect [10]. This type of variation occurs due to the negative surface tension coefficient of the surface oxide as compared to underlying metal. Additionally, as mentioned above, formation of $Mg(OH)_2$ in addition to $Al(OH)_3$ in reused powder will increase the overall hydrogen content in the alloy, which can also contribute towards increase in porosity in as-built material. The effect of oxide and hydroxide formation during powder reuse on porosity appearance and mechanical properties will be discussed in the following study for the same materials by authors.

4. Conclusions

Powder degradation during laser powder bed fusion of AlSi10Mg powder for 30 months has been evaluated. The analysis of the powder surface morphology showed presence of the spatter particles with characteristic nodular surface oxide scale covering powder particles and formed during the melting and solidification in the machine environment. The quantification of spatter particles showed an increase in volume fraction of spatters up to around 3 % in the powder reused for 30 months, which is quite significant considering the thickness of oxide scale which lies in the range of 50-125 nm. The STEM+EDX analysis verified the presence of wavy nodular structure of the surface oxide scale on the sputters, composed of Al and Mg based oxides. XPS analysis confirms formation of thick surface oxide, predominantly formed by Al_2O_3 with the presence of the $MgAl_2O_4$ spinel on the top oxide surface. Thermodynamic calculations on oxide formation for the alloy of interest reaffirmed the findings of XPS and STEM-EDX analysis regarding the formation of $MgAl_2O_4$ spinel and Al_2O_3 (corundum) during solidification of spatter particles in the simulated environment. Furthermore, XPS results showed an overall increase in average oxide layer thickness from 4 nm in virgin powder to 38 nm in the reused powder, in agreement with the increase in bulk oxygen content in reused powder from 500 ppm to 1250 ppm. Hence, a better control of oxygen partial pressure in the build chamber is required to reduce the extent of oxidation of spatter particles and hence powder degradation. Results indicate that periodical monitoring of the powder feedstock during multiply LB-PBF manufacturing is required to assure necessary quality of the feedstock powder and hence defect-free components.

Contributions

Ahmad Raza planned and administered the experiments with assistance of Tobias Fiegl, and supervision of Eduard Hryha. He further analyzed results and wrote manuscript. Tobias Fiegl, Martin Franke and Carolin Körner were involved in ageing of powder and sample collection for the analysis from X LINE 2000R is used in Fürht at NMF, FAU Erlangen, Germany. Imran Hanif assisted in FIB sample preparation, TEM experimentation and analysis. Andreas Markström provided his assistance in Thermo-Calc calculations and analysis in draft. Eduard Hryha closely supervised the experimentation, assisted in analysis, and further contributed in revisions of the Manuscript.

Credit author statement

Ahmad Raza planned and administered the experiments with assistance of Tobias Fiegl, and supervision of Eduard Hryha. He further analyzed results and wrote manuscript. Tobias Fiegl, Martin Franke and Carolin Körner were involved in ageing of powder and sample collection for the analysis from X LINE 2000R is used in Fürht at NMF, FAU Erlangen, Germany. Imran Hanif assisted in FIB sample preparation, TEM experimentation and analysis. Andreas Markström provided his assistance in Thermo-Calc calculations and analysis in draft. Eduard Hryha closely supervised the experimentation, assisted in analysis, and further contributed in revisions of the Manuscript.

Declaration of Competing Interest

The authors declare that they have no known competing financial interests or personal relationships that could have appeared to influence the work reported in this paper.

Acknowledgement

This work has been conducted in the framework of the Centre for Additive Manufacturing – Metal (CAM^2) supported by the Swedish Governmental Agency of Innovation Systems (Vinnova). Additional support from the strategic innovation program

LIGHTer, provided by Vinnova, and Production Area of Advance at Chalmers University of Technology is gratefully acknowledged.

Appendix A. Supplementary data

Supplementary data to this article can be found online at https://doi.org/10.1016/j.matdes.2020.109358.

References

[1] A.N.D. Gasper, et al., Oxide and spatter powder formation during laser powder bed fusion of Hastelloy X, Powder Technol. 354 (2019) 333–337.
[2] A. Aversa, et al., New aluminum alloys specifically designed for laser powder bed fusion: A review, Materials 12 (7) (2019).
[3] L. Thijs, K. Kempen, J.P. Kruth, J. Van Humbeeck, Fine-structured aluminium products with controllable texture by selective laser melting of pre-alloyed AlSi10Mg powder, Acta Mater. 61 (5) (2013) 1809–1819.
[4] K. Kempen, L. Thijs, J. Van Humbeeck, J.P. Kruth, Processing AlSi10Mg by selective laser melting: Parameter optimisation and material characterisation, Mater. Sci. Technol. (United Kingdom) 31 (8) (2015) 917–923.
[5] F. Ahmed, et al., Study of powder recycling and its effect on printed parts during laser powder-bed fusion of 17-4 PH stainless steel, J. Mater. Process. Technol. 278 (2019) (2020) 116522.
[6] E. Santecchia, S. Spigarelli, M. Cabibbo, Material reuse in laser powder bed fusion: Side effects of the laser—metal powder interaction, Metals 10 (3) (2020) 1–21.
[7] H. Gruber, P. Karimi, E. Hryha, L. Nyborg, Effect of Powder Recycling on the Fracture Behavior of Electron Beam Melted Alloy 718, Powder Metall. Prog. 18 (1) (2018) 40–48.
[8] C. Pauzon, E. Hryha, P. Forêt, L. Nyborg, Effect of argon and nitrogen atmospheres on the properties of stainless steel 316 L parts produced by laser-powder bed fusion, Mater. Des. 179 (2019) 107873.
[9] C. Pauzon, P. Forêt, E. Hryha, T. Arunprasad, L. Nyborg, Argon-helium mixtures as Laser-Powder Bed Fusion atmospheres: Towards increased build rate of Ti-6Al-4V, J. Mater. Process. Technol 279 (2020) 116555.
[10] C.L.A. Leung, S. Marussi, M. Towrie, R.C. Atwood, P.J. Withers, P.D. Lee, The effect of powder oxidation on defect formation in laser additive manufacturing, Acta Mater. 166 (2019) 294–305.
[11] S. Ly, A.M. Rubenchik, S.A. Khairallah, G. Guss, M.J. Matthews, Metal vapor micro-jet controls material redistribution in laser powder bed fusion additive manufacturing, Sci. Rep. 7 (1) (2017) 1–12.
[12] M.J. Matthews, G. Guss, S.A. Khairallah, A.M. Rubenchik, P.J. Depond, W.E. King, Denudation of metal powder layers in laser powder bed fusion processes, Acta Mater. 114 (2016) 33–42.
[13] A. Bin Anwar, Q.C. Pham, Study of the spatter distribution on the powder bed during selective laser melting, Addit. Manuf. 22 (2018) 86–97.
[14] C. Pauzon, E. Hryha, P. Forêt, L. Nyborg, Effect of argon and nitrogen atmospheres on the properties of stainless steel 316 L parts produced by laser-powder bed fusion, Mater. Des. 179 (2019).
[15] V. Gunenthiram, et al., Experimental analysis of spatter generation and melt-pool behavior during the powder bed laser beam melting process, J. Mater. Process. Technol 251 (2018) 376–386.
[16] M.J. Heiden, et al., Evolution of 316L stainless steel feedstock due to laser powder bed fusion process, Addit. Manuf 25 (2019) 84–103.
[17] L.C. Ardila, et al., Effect of IN718 recycled powder reuse on properties of parts manufactured by means of Selective Laser Melting, Physics Procedia 56 (2014) 99–107.
[18] H. Gruber, M. Henriksson, E. Hryha, L. Nyborg, Effect of Powder Recycling in Electron Beam Melting on the Surface Chemistry of Alloy 718 Powder, Metall. Mater. Trans. A Phys. Metall. Mater. Sci. 50 (9) (2019) 4410–4422.
[19] A.T. Sutton, C.S. Kriewall, S. Karnati, M.C. Leu, J.W. Newkirk, Characterization of AISI 304L stainless steel powder recycled in the laser powder-bed fusion process, Addit. Manuf. 32 (2020) 100981.
[20] P.E. Carrion, A. Soltani-Tehrani, S.M. Thompson, N. Shamsaei, Effect of powder degradation on the fatigue behavior of additively manufactured as-built Ti-6Al-4V, Solid Freeform Fabrication 2018: Proceedings of the 29th Annual International Solid Freeform Fabrication Symposium - An Additive Manufacturing Conference, SFF 2018 2020, pp. 1366–1372.

[21] L. Cordova, M. Campos, T. Tinga, Revealing the Effects of Powder Reuse for Selective Laser Melting by Powder Characterization, JOM 71 (3) (2019) 1062–1072.
[22] A. Montelione, S. Ghods, R. Schur, C. Wisdom, D. Arola, M. Ramulu, Powder Reuse in Electron Beam Melting Additive Manufacturing of Ti6Al4V: Particle Microstructure, Oxygen Content and Mechanical Properties, Addit. Manuf. 35 (December 2019) (2020) 101216.
[23] J.O. Andersson, T. Helander, L. Höglund, P. Shi, B. Sundman, Thermo-Calc & DICTRA, computational tools for materials science, Calphad Comput. Coupling Phase Diagrams Thermochem. 26 (2) (2002) 273–312.
[24] V. Seyda, N. Kaufmann, C. Emmelmann, Investigation of Aging Processes of Ti-6Al-4 v Powder Material in Laser Melting, Physics Procedia 39 (2012) 425–431.
[25] M. Simonelli, et al., A Study on the Laser Spatter and the Oxidation Reactions During Selective Laser Melting of 316L Stainless Steel, Al-Si10-Mg, and Ti-6Al-4V, Metall. Mater. Trans. A Phys. Metall. Mater. Sci. 46 (9) (2015) 3842–3851.
[26] E. Hryha, R. Shvab, H. Gruber, A. Leicht, L. Nyborg, Surface oxide state on metal powder and its changes during additive manufacturing: An overview, Proceedings Euro PM 2017: International Powder Metallurgy Congress and Exhibition, 2018.
[27] E. Hryha, E. Dudrova, L. Nyborg, On-line control of processing atmospheres for proper sintering of oxidation-sensitive PM steels, J. Mater. Process. Technol. 212 (4) (2012) 977–987.
[28] C. Oikonomou, D. Nikas, E. Hryha, L. Nyborg, Evaluation of the thickness and roughness of homogeneous surface layers on spherical and irregular powder particles, Surf. Interface Anal. 46 (10–11) (2014) 1028–1032.
[29] K. Zumsande, et al., Characterization of the surface of Fe-19Mn-18Cr-C-N during heat treatment in a high vacuum - An XPS study, Mater. Charact. 71 (2012) 66–76.
[30] E. Hryha, C. Gierl, L. Nyborg, H. Danninger, E. Dudrova, Surface composition of the steel powders pre-alloyed with manganese, Appl. Surf. Sci. 256 (12) (2010) 3946–3961.
[31] C. Oikonomou, E. Hryha, L. Nyborg, Development of methodology for surface analysis of soft magnetic composite powders, Surf. Interface Anal. 44 (8) (2012) 1166–1170.
[32] D. Riabov, E. Hryha, M. Rashidi, S. Bengtsson, L. Nyborg, Effect of atomization on surface oxide composition in 316L stainless steel powders for additive manufacturing, Surf. Interface Anal. 52 (11) (2020) 694–706.
[33] G. Al, J.A. Rotole, P.M.A. Sherwood, J.A. Rotole, P.M.A. Sherwood, Gibbsite (α- Al(OH) 3) by XPS, vol. 25, 1998.
[34] J.F. Moulder, W.F. Stickle, P.E. Sobol, K.D. Bomben, Handbook of X-ray photoelectron spectroscopy: a reference book of standard spectra for identification and interpretation of XPS data: Physical Electronics, Eden Prairie, MN, 1995, 2000 261.
[35] B.A. Taleatu, et al., XPS and some surface characterizations of electrodeposited MgO nanostructure, Surf. Interface Anal. 46 (6) (2014) 372–377.
[36] P. Marcus, C. Hinnen, I. Olefjord, Determination of attenuation lengths of photoelectrons in aluminium and aluminium oxide by angle-dependent x-ray photoelectron spectroscopy, Surf. Interface Anal. 20 (11) (1993) 923–929.
[37] E. Hryha, R. Shvab, M. Bram, M. Bitzer, L. Nyborg, Surface chemical state of Ti powders and its alloys: Effect of storage conditions and alloy composition, Appl. Surf. Sci. 388 (2016) 294–303.
[38] H.L. Lukas, S.G. Fries, B. Sundman, Computational thermodynamics: The Calphad method, 9780521868 2007.
[39] K. Djebaili, Z. Mekhalif, A. Boumaza, A. Djelloul, Xps, Ftir,Edx,Xrd Analysis of Al2O3 Scales Grown on Pm2000 Alloy, J. Spectrosc. (2015) 1–16, 2013.
[40] F. Trevisan, et al., On the selective laser melting (SLM) of the AlSi10Mg alloy: Process, microstructure, and mechanical properties, Materials 10 (1) (2017).